Sea Ice Simulations Based on Fields Generated by the GLAS GCM

CLAIRE L. PARKINSON

Laboratory for Atmospheric Sciences, NASA, Goddard Space Flight Center, Greenbelt, MD 20771

GERALD F. HERMAN[1]

Department of Meteorology, University of Wisconsin, Madison, 53706

(Manuscript received 19 May 1980, in final form 16 September 1980)

ABSTRACT

A four-month simulation of the thermodynamic portion of the Parkinson-Washington sea ice model was conducted using atmospheric boundary conditions that were obtained from a pre-computed seasonal simulation of the Goddard Laboratory for Atmospheric Sciences' General Circulation Model (GLAS GCM). The sea ice thickness and distribution were predicted for the 1 January–30 April period based on the GCM-generated fields of solar and infrared radiation, specific humidity and air temperature at the surface, and snow accumulation. The sensible heat and evaporative fluxes at the surface are mutually consistent with the ground temperatures generated by the ice model and the air temperatures generated by the atmospheric model.

In general, in the Northern Hemisphere the predicted ice distributions and the wintertime accretion and southward advance of the pack ice are well simulated. The computed ice thickness in the Southern Hemisphere appears reasonable, but the Antarctic melt season is extended, causing ice coverage to be less than observed in late March and April. During the Northern Hemisphere winter, the simulated ice accretion is the result of the net deficit of longwave radiation, heat gained from the ocean, and sensible heat lost to the atmosphere. In the early part of the Southern Hemisphere summer, the melting essentially balances the excess of solar over longwave radiation at the surface, while later in the simulation accretion balances the longwave and convective heat losses.

The results show that the Parkinson–Washington sea ice model produces acceptable ice concentrations and thicknesses when used in conjunction with the GLAS GCM for the January to April transition period. These results suggest the feasibility of fully coupled ice-atmosphere simulations with these two models.

1. Introduction

A frequently-cited goal in both general circulation studies and cryospheric research is the realistic modeling of the true interaction between sea ice processes and atmospheric processes. The relationship between the variations in the geographical distribution and physical properties of sea ice and the variations in the large-scale atmospheric circulation is obviously very complicated. Wind stress at the upper surface of the pack ice has long been accepted as the principal motive force for pack ice drift, while the energy balance and resultant ice temperature or rate of melting at the surface depend on atmospheric temperature, humidity, radiation and precipitation. At the same time, the fluctuations in the distribution and properties of sea ice may themselves be the cause of a range of atmospheric variations. The statistical relationship between ice and atmospheric processes has been well established through the observational analyses of Walsh and Johnson (1979) and others. Presumably the exact nature of the physical relationships will emerge from carefully designed modeling experiments in conjunction with data-based studies.

The study of the large-scale relationships between the sea ice and the atmosphere through numerical methods has thus far involved models which can be classified into three broad categories: (1) Sea ice models which depend upon but do not alter the atmospheric forcings (e.g., stress or radiation) that are specified from observational data or from atmospheric models; (2) Atmospheric models in which sea ice is a prescribed lower boundary condition that remains independent of the simulated atmospheric fields; (3) Fully coupled ice-atmosphere models in which the ice distribution and atmospheric fluxes are determined in a mutually consistent fashion.

In the first of these, which may be termed *non-interactive ice models*, the motion and thickness of sea ice are calculated from time-dependent mechanical and thermodynamic equations which require as boundary conditions such variables as the stress and the turbulent and radiative energy fluxes at the ice-atmosphere interface and at the ice-ocean interface.

[1] Also NASA Goddard Laboratory for Atmospheric Sciences.

0027-0644/80/122080-12$07.00

TABLE 1. Summary of large-scale sea ice models.

Model	Description	Required atmospheric parameters
1. Hibler (1979)	Dynamic with specified thermodynamics; simulation for full yearly cycle; Arctic Basin	Surface pressure; specified thermodynamic growth rates
2. Kulakov *et al.* (unpublished)	Dynamic-thermodynamic; 1 month simulation; South Polar region	Surface air temperature, pressure, and total radiation
3. Ling *et al.* (1980)	Dynamic; 18-day simulation; Weddell Sea	Surface air pressure
4. Parkinson and Washington (1979)	Dynamic-thermodynamic; simulation for full yearly cycle; North and South Polar regions	Surface air temperature, dew point, and geostrophic wind velocity
5. Pritchard *et al.* (1977)	Dynamic-thermodynamic; 10-day simulation; portion of Beaufort Sea	Surface air pressure
6. Rothrock (1975)	Dynamic; simulation for long-term average conditions; Arctic Basin	Surface air pressure
7. Washington *et al.* (1976)	Thermodynamic; simulation for full yearly cycle; North and South Polar regions	Surface air temperature, dew point, and geostrophic wind speed

In these models the changing character of the ice field does not alter the atmospheric forcing at the boundary, and consequently some of the conditions may be viewed as unrealistic, since the forcing may be inconsistent with the actual state of the ice. As an example, the stress at the surface depends upon the surface geostrophic wind and the drag characteristics of the ice; but in a non-interactive ice model the stress field would generally not readjust to the changing ice conditions. A summary of major large-scale ice models together with their required atmospheric inputs is given in Table 1.

In the second set of models, which we term *non-interactive atmospheric models*, the effective pack ice distribution is usually realized through the specified surface emissivity and reflectivity required in the atmospheric radiation calculations, through the temperature and wetness of the surface in thermodynamic calculations, and through the surface roughness in the horizontal momentum equation. The distribution and properties of the ice may vary with time according to a predetermined climatology, but they remain independent of the model-generated fields. Most operational weather forecasting models, and most versions of current GCMs (Table 2) are non-interactive with respect to sea ice.

Non-interactive atmospheric models have been used in a number of investigations of the role of sea ice in global climate. These include the ice-free Arctic Ocean experiments of Warshaw and Rapp (1973), the ice age experiments of Williams *et al.* (1974), and the marginal ice zone experiments of Herman and Johnson (1978). It is sometimes noted that in these experiments the simulated effect of the sea ice may be somewhat exaggerated because the experiments contain no ice-atmosphere feedback. For example, if the principal effect of reducing sea ice concentration is to increase the transfer of sensible heat to the atmosphere, then in nature a negative feedback is involved because the cooling of the ocean surface due to its heat loss to the atmosphere may be large enough to cause more ice to accrete. There is a positive feedback as well, involving the reflectivity of sea ice and the surface energy balance and surface temperature.

Fully coupled ice-atmosphere models, the third category listed above, allow the distribution of sea ice to evolve as part of the solution to the complete system of equations governing atmospheric and sea ice processes. A wide range of highly parameterized climate models fall into this category (for a review, see Saltzman, 1978); but, so far, there have been very few experiments with fully coupled ice-atmos-

TABLE 2. Sea ice specification in general circulation models.

Model	Treatment
1. GLAS (Halem *et al.*, 1979)	Fixed 3 m slab; specified variation of margin
2. GFDL (Manabe and Wetherald, 1980)	Occurrence depends on surface energy balance of ocean
3. GFDL-coupled (Manabe *et al.*, 1979)	Thickness and concentration depend on energy balance of ocean surface layer
4. NCAR (Washington and Williamson, 1977)	Specified January and July margin affecting only shortwave albedo
5. NCAR (Washington *et al.*, 1980)	Varies according to 1-dimensional energy balance model
6. Oregon State/UCLA (Schlesinger and Gates, 1979)	Fixed 3 m slab with prescribed margin variations
7. Meteorology Office (Corby *et al.*, 1972)	Prescribed slab

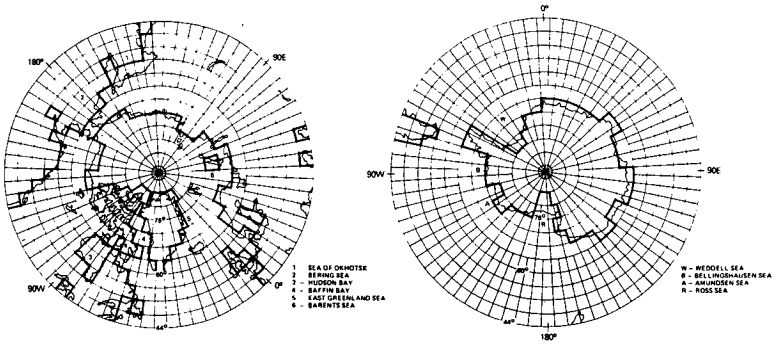

FIG. 1. Grid structure. Heavy solid line indicates the model resolution of continental boundaries.

phere general circulation models. The results of recent experiments with the coupled ice-atmosphere-ocean model at the Geophysical Fluid Dynamics Laboratory (GFDL) (Manabe *et al.*, 1975) have illustrated some of the difficulties. There, for example, the reduction in surface albedo due to melting sea ice caused anomalous heating in the south polar regions, while excessive ice growth in the Arctic, along with the absence of leads, limited the amount of heat that was conducted to the surface. This excessive growth was eliminated in later versions (Manabe *et al.*, 1979) in which the mean annual solar radiation was replaced with a realistic seasonal cycle. At the National Center for Atmospheric Research (NCAR), an *asynchronous coupling* has been performed with atmosphere, ocean and ice models. The atmospheric model was run individually for January, April, July and October; the resulting data were fitted to an annual curve which then drove the ocean model for a 5-year simulation; the new sea surface temperature and sea ice distributions were then used as revised boundary conditions for the atmospheric calculations. In general the sea ice distributions resulting from the simulation were thinner and less extensive than the observed (Washington *et al.*, 1980).

It is quite possible that one of the reasons that the fully non-interactive GCMs perform as well as they do in polar regions (e.g., Herman and Johnson, 1980) lies in their climatologically fixed sea ice margins and ocean temperatures and in the constraint which these place on the radiative and convective fluxes at the surface. It is thus not entirely unexpected that the first attempts at coupled simulations have produced additional difficulties.

The results reported here represent a preliminary step in assessing the feasibility of coupled ice-atmosphere simulations. This work is designed to demonstrate whether the thermodynamic portion of the sea ice model of Parkinson and Washington (1979) can predict a realistic seasonal variation of ice thickness and ice concentration when forced by the fields generated by a seasonal simulation with the GCM of the Goddard Laboratory for Atmospheric Sciences. It is important to note that we have not conducted a fully-coupled experiment, but rather have forced a non-interactive ice model with the precomputed results of a non-interactive GCM. A principal difficulty lies in assessing whether the success or failure of the results should be attributed to the atmospheric GCM or to the sea ice model and whether specific deficiencies will be reduced or enhanced when the two models are actually coupled.

2. Summary of models

The model calculations are carried out on the grid of the GLAS GCM. Horizontal grid resolution is defined by 5° longitude and 4° latitude spacing, with the grid squares centered at longitudes 0°, 5°E, . . . , 355°E and at latitudes 90°S, . . . , 6°S, 2°S, 2°N, 6°N, . . . , 90°N. This yields a grid size of 72 × 46 for the globe.

The current version of the GLAS GCM incorporates a *split grid* at high latitudes, with the longitudinal resolution doubled to 10° for latitudes 64–80° and doubled again to 20° for latitudes poleward of 80° (Fig. 1). For the sea ice calculations we have retained the full 72 × 46 grid size, and have interpolated the GCM grid point values to the off-split grid points.

a. Thermodynamic sea ice model

The sea ice model employed for the simulations is a thermodynamic model which calculates a lead percentage within the ice but does not simulate ice dynamics. It is essentially the thermodynamic portion of the three-dimensional model of Parkinson and Washington (1979), a model based in part on the one-dimensional models of Maykut and Untersteiner (1971) and of Semtner (1976). The Parkinson

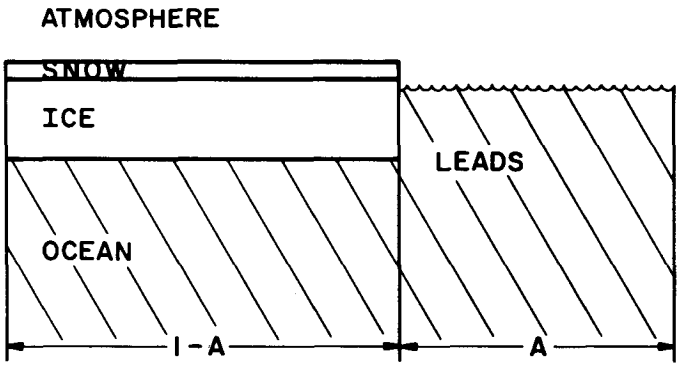

FIG. 2. Schematic of major divisions within a grid element.

and Washington model was developed for and run previously with mean monthly climatological data as input, contrasting with the GCM-generated data used here. The results of the climatological simulation can be found in Parkinson and Washington. Note that we are assuming that a reasonable simulation of ice thickness and distribution can be obtained when the details of ice dynamics and mechanics are explicitly neglected. This assumption is supported by the results of Parkinson and Washington, which show that the insertion of the dynamics did not substantially alter the model results from an earlier, strictly thermodynamic simulation.

Fig. 2 illustrates the basic model elements at an individual grid square. Uniform ice and snow layers cover a portion of the area, with the remainder covered by leads or open water. The fractional area A of leads and the thicknesses of the ice and snow are time dependent, being recalculated at each of the 6-hourly time steps. Depending on time and location, the snow layer or both the ice and snow layers may be non-existent.

The calculations for thickness changes are based on energy balances at the various interfaces. The fluxes between the upper snow surface and the atmosphere are sensible and latent heat H and LE respectively, incoming longwave radiation LW, incoming shortwave radiation SW, and emitted longwave radiation from the surface to the atmosphere. The only fluxes through the ice and snow are conductive, and there is also a flux to the undersurface of the ice from the ocean, F_0.

Formation of energy balances at the air-snow and snow-ice interfaces yields the pair of equations:

$$H + LE + \epsilon LW + (1 - \alpha)SW + \epsilon\sigma T_{sfc}^4 + \frac{k_s}{h_s}(T_I - T_{sfc}) = 0 \quad (1)$$

$$\frac{k_s}{h_s}(T_I - T_{sfc}) = \frac{k_I}{h_I}(T_B - T_I) \quad (2)$$

where ϵ is the longwave emissivity and α the shortwave albedo of snow; σ is the Stefan-Boltzmann constant; T_{sfc}, T_I and T_B are the temperatures at the upper snow surface, the snow-ice interface and the bottom ice surface respectively; k_s, k_I are the conductivities of the snow and ice respectively; and h_s, h_I are the snow and ice layer thicknesses.

Eqs. (1) and (2) are solved for T_I and T_{sfc}. If the calculated value of T_{sfc} exceeds the freezing point, the surface temperature is set exactly at freezing and the remaining energy is used to melt a portion of the snow. Otherwise, the snow thickness is increased by the snowfall amount obtained from the GCM.

At the bottom surface of the ice, the amount of ablation or accretion is calculated by balancing the energy flux from this change of state with the ocean heat flux and the conductive flux. This results in the following thickness change:

$$\Delta h_I = \frac{\Delta t}{Q_I}\left[\frac{k_I}{h_I}(T_B - T_I) - F_0\right] \quad (3)$$

where Δt is the time step (equal to 6 h) and Q_I is the heat of fusion of ice.

In grid squares where no ice exists or where ice exists but without a snow cover, the calculations are similarly based on energy balances, although with the following adjustments. In the case of no ice, the net energy flux into the ocean mixed layer is used to adjust the water temperature, with a small amount of ice being formed when the temperature reaches freezing; no account is taken of heat transport in the ocean or local upwelling effects. In the case of ice with no snow cover, the surface energy balance is constructed similarly to Eq. (1), with a modification to account for the penetration of shortwave radiation into the ice. Details are provided in Parkinson and Washington.

The lead percentage is parameterized by calculating the net energy input into the lead and distributing this energy to the lead itself and to the surrounding ice. In the event of a positive net input, the energy heats the water and laterally melts the ice, with the

partition of energy being proportional to the lead area. In the event of a negative net input (energy loss), the energy deficit is balanced by cooling the water, and, if the water temperature reaches freezing, then by laterally accreting new ice onto the existing ice.

b. The GLAS General Circulation Model

The principal features of the GLAS General Circulation Model have been described by Somerville *et al.* (1974), Stone *et al.* (1977), and Halem *et al.* (1979). Aspects of the model which are particularly relevant for high latitude studies have been discussed by Herman and Johnson (1978, 1980). Here it suffices to note that the GLAS GCM is a primitive equation model utilizing a sigma vertical coordinate system and 4° latitude by 5° longitude horizontal spacing. Computational stability at high latitudes is ensured through the use of the split grid; heat and moisture fluxes at the surface are computed through simple drag laws; and sea surface temperatures and sea ice margins are specified to vary smoothly according to a predetermined climatology.

More specifically, for the radiative fluxes needed in the present experiment, the GCM solar radiation is determined by the 2-stream calculation of Lacis and Hansen (1974) and the longwave radiation is based on an algorithm developed by Wu and Kaplan (Wu, 1980). The Lacis and Hansen formulation includes a detailed representation of atmospheric absorption and scattering, while the Wu and Kaplan formulation includes 10 regions in the water vapor spectrum. Both radiation calculations are fully interactive with the model-generated distributions of water vapor, cloudiness, and surface albedo. These radiation calculations are considerably more elaborate than those used when the sea ice model was run independently of the GCM (cf. Parkinson and Washington).

The simulated polar climatology of the GLAS GCM is discussed in detail by Herman and Johnson (1980). In the Arctic and peripheral Arctic oceans the simulated wintertime distributions of sea level pressure and surface energy fluxes are realistic, although surface air temperatures are 5–9°C too warm. Over the peripheral Antarctic oceans the belt of low pressure centers around the continent is not simulated as a result of the GCM's difficulty in simulating baroclinic eddy activity in the high latitudes of the Southern Hemisphere. Temperatures and energy fluxes are not unreasonable, although validation is difficult because of the lack of observed data.

3. Description of experiment

The fields needed for the ice calculations (Section 2a) are sensible and latent heat, longwave and shortwave radiation incident at the surface, and snowfall. The incoming longwave, incoming shortwave, and precipitation terms are taken directly from fields generated by the GCM, while the sensible and latent heat terms are calculated by bulk aerodynamic formulae which require from the GCM values for surface air temperature, wind speed, and surface specific humidity. These fields are entered into the calculations at each ice model timestep, i.e., every 6 h.

The GCM fields were generated by a 4-month simulation initialized from NMC conditions at 00 GMT 1 January 1975. The principal features of this simulation (GLAS Reference No. D122) have been analyzed in detail by Halem *et al.* (1979).

The ice model requires initial conditions for sea ice concentrations and thicknesses, and for the surface temperatures of the ocean, ice and snow. The initial ice concentrations were approximated from maps of average brightness temperature recorded by the Electronically Scanning Microwave Radiometer (ESMR) on Nimbus 5 over the 3-day period 30 December 1974–1 January 1975. A description of the ESMR data set is provided in Zwally and Gloersen (1977). As satellite data is not yet able to provide thickness estimates, the initial thickness distributions were estimated based on climatology. These initial ice conditions are mapped in Fig. 3. The initial ocean surface temperature at each grid square is either the initial GCM ocean temperature or the freezing point of sea water, whichever is larger; while the initial snow and ice surface temperatures are either the initial GCM snow and ice temperatures or the freezing point, whichever is smaller.

It is important to note that while the initial conditions for the GCM and the ice are based on January 1975 data, the present experiment is not designed to predict 1975 ice conditions. It is commonly accepted that, after some period of time ranging from several days to several weeks, the simulated GCM fields become essentially independent of the prescribed initial state, and more characteristic of the model's internal dynamical adjustment to the boundary conditions and external forcing. Thus, it is more correct to consider the sea ice model as being forced by the GLAS model climatology, rather than by a simulated 1975 atmospheric circulation.

It also follows that since the model-generated fields result in part from the GCM's adjustment to the boundary conditions (e.g., sea surface temperature, ice margin, surface albedo), the various atmospheric fields that force the sea ice model will actually contain some structure that is determined by the observed climatological surface boundary conditions. The computed sea ice fields thus may be anchored to an uncertain degree to the climatological ice conditions through the GCM's distribu-

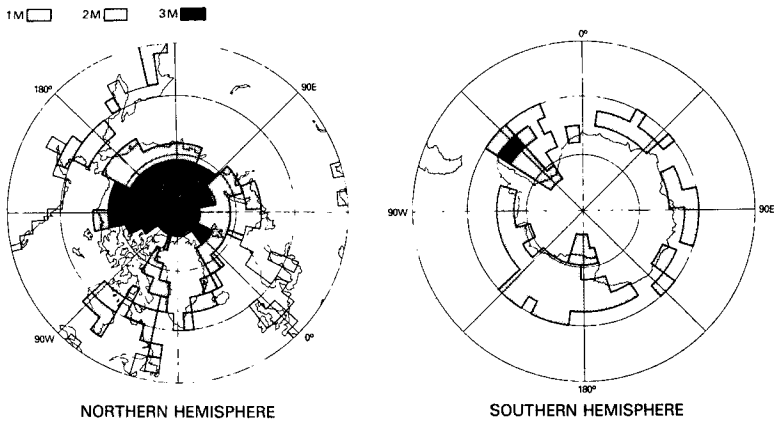

FIG. 3. Initial ice thickness (m) on 1 January.

tion of precipitation, radiation, etc. The effect of all of the physical processes which determine the distribution of sea ice in nature, including large-scale ice and ocean dynamics, is thereby implicitly communicated by the GCM to the sea ice model.

4. Results and discussion

a. Spatial fields of ice thickness and concentration

Selected results of the simulation are shown in Figs. 4–7. The Northern Hemisphere ice extents slowly move equatorward from January to March, first expanding southward in the Sea of Okhotsk in early January, then in the western Bering and Barents seas in late January. In February the extent is stable both in the Sea of Okhotsk and to the east of Greenland; there is a slight advance to the southwest of Greenland, and there are small regions of advance compensated by small regions of retreat in both the Bering and Barents seas. The ice begins its retreat in the Okhotsk and Bering seas in March and is in retreat in all sectors during April (Figs. 3–7).

To the extent that 1975 ice conditions are representative of climatology, it is possible to use 1975 data from the ESMR on Nimbus 5 to evaluate broad aspects of the ice model's simulation. The overall simulated distribution of Northern Hemisphere ice corresponds fairly well with the observed. However, there are discrepancies between the observations and the simulation. For instance, in the Sea of Okhotsk the observed ice advance occurs predominantly in February rather than in January, though the maximum extent in both cases is reached in early March, with some slight retreat in late March. The simulated full ice cover through April in Hudson Bay is confirmed in the observations, although the observations do not confirm as extensive an ice cover as is simulated in February in the Barents Sea. The situation in the Barents Sea can probably be explained by the failure to represent the warm, northward flowing ocean current to the west of Scandinavia.

In the Southern Hemisphere, the simulated ice edge remains steady for the first half of January, then in the latter half of January retreats significantly around most of the Antarctic continent except in the Weddell and Bellingshausen seas. There

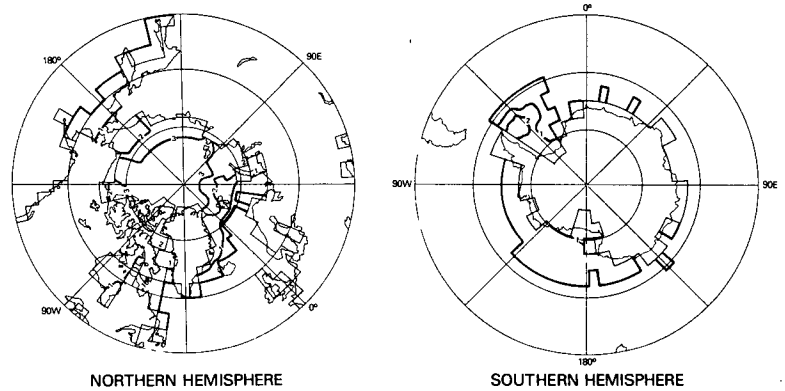

FIG. 4. Simulated ice thickness (m) on 1 February. Heavy lines show the ice edge and contours of ice thickness. Lighter lines show the continental boundaries and grid resolution of those boundaries.

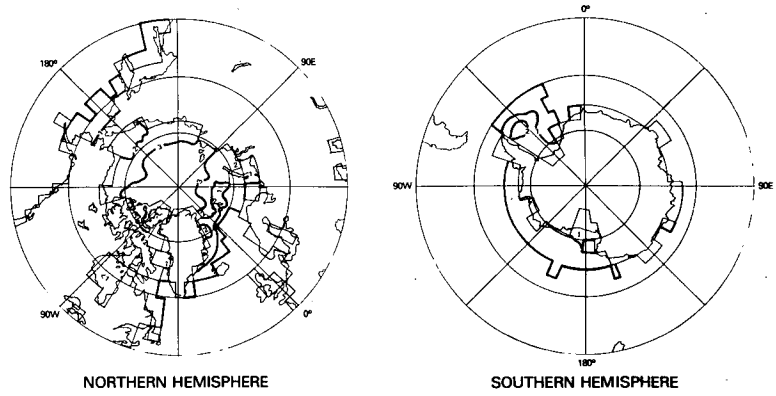

FIG. 5. Simulated ice thickness (m) on 1 March.

is continued retreat of the little ice remaining off the coast of East Antarctica during February, with essentially no East Antarctic ice left by 1 March. In February there is also continued edge retreat to the north and northeast of the Ross Sea, though the edge positions in the Weddell and Bellingshausen seas are maintained. In March the East Antarctic situation remains stable with practically no ice; the Bellingshausen Sea still shows no change in ice extent; and both the Ross and Weddell seas lose some ice in their northernmost regions and gain some in their southernmost regions. During April there is no further edge retreat in any region and there is significant expansion around the coast of East Antarctica and in the Weddell Sea (Figs. 3–7).

The 1975 ESMR imagery (unpublished) for the Southern Hemisphere confirms the relatively stable position of the ice edge in early January and the ice retreat in the East Antarctic and Ross Sea during late January and during February. However, the ESMR observations also indicate considerable ice advance during March, which would suggest a model delay of ½–1 month in the start of the fall growth season. A likely cause of this delay may be the unrealistically high surface air temperatures which characterize the GLAS GCM's Antarctic climatology. For instance, in mid-February, the 270 K isotherm of the GCM values closely follows the Antarctic coastline around most of the continent, the major exception occurring in the Weddell Sea, where the contour is further north than the coast. Thus, with the exception of the Weddell Sea, very little of the model's Southern Ocean is overlain by air with temperatures below 270 K. Based on observed climatological averages for the month of February, these simulated temperatures would be anomalously warm and thus would explain the delay in the refreezing of the surface water.

For more detail on the simulated ice thickness and concentration values, the time sequences of these quantities are tabulated in Table 3 for three specific regions: the Weddell Sea in the Southern Hemisphere and the East Greenland Sea and Central Arctic Basin in the Northern Hemisphere. The calculations for Table 3 involved all grid squares which contained ice irrespective of its concentration. The concentration value listed is the average value for the ice-laden grid squares, and the thickness listed is the average ice thickness, without regard to concentration.

In the Weddell Sea, the concentrations and thick-

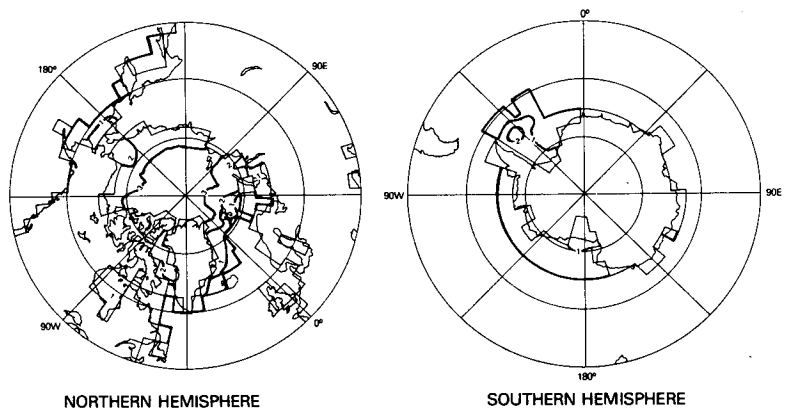

FIG. 6. Simulated ice thickness (m) on 1 April.

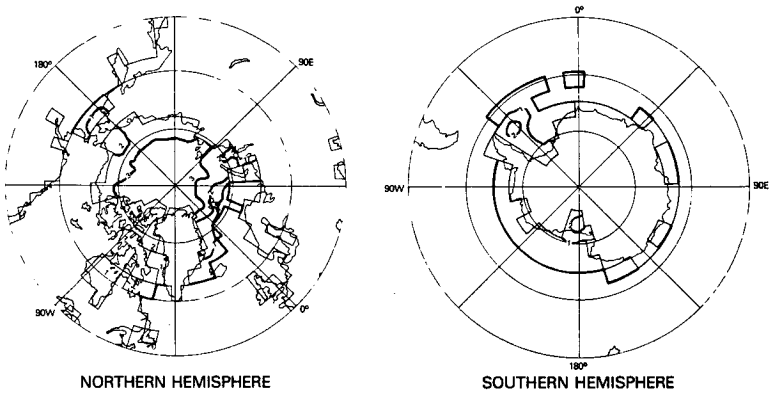

FIG. 7. Simulated ice thickness (m) on 29 April.

nesses steadily decrease during January and February as expected for the summer melt period. Two grid squares lose their ice cover in early March, with the result that the minimum ice extent occurs in mid-March. The ESMR satellite imagery for all four years available (1973–76) shows a slight increase in ice extent from the start to the middle of the month, suggesting that the numerical model has extended the summer melt period about 2 weeks beyond what the observations would indicate. For the month and a half after 15 March, the simulated ice concentrations rapidly increase, as would be expected for this early fall season. The thickness decreases from 15 March to 15 April, a result of averaging into the calculations newly ice-laden grid squares with very thin ice covers.

In the Central Arctic, averaged ice concentrations are initialized at 98.8%, increase to 99.5% by mid-February and then remain at this maximum-allowable value for the remainder of the simulation. The central Arctic thickness values slowly increase over the four-month simulation. These results are in general agreement with the expected trends for the central Arctic region.

The East Greenland Sea situation is somewhat more complicated since the number of grid squares involved changes over the simulation period. The increase in area of ice-laden waters from 1–15 January can easily account for the decrease in average ice thickness from 1.62 to 1.51 m. However, the continued, though less rapid, decrease in thickness through the end of March cannot be so explained, and this is presumably an unrealistic result. By contrast, the increase in ice concentration over the same period is reasonable.

b. Regionally-averaged energy balances

We illustrate in Figs. 8–10 the evolution of the areal averages of the principal GCM-generated parameters to which the ice model responds, and of the main components of the surface energy and mass balance. The GCM communicates to the ice model precipitation (i.e., snowfall), surface air temperature, specific humidity, and solar and incoming longwave radiation, the latter two variables being functions of ambient cloudiness. Evaporation and sensible heat exchange at the surface are based on GCM-generated

TABLE 3. Regionally-averaged ice thickness and concentration.

	Weddell Sea			East Greenland Sea			Central Arctic		
Date	Area of ice-laden waters (10^6 km^2)	Concentration (%)	Thickness (m)	Area of ice-laden waters (10^6 km^2)	Concentration (%)	Thickness (m)	Area of ice-laden waters (10^6 km^2)	Concentration (%)	Thickness (m)
1 January	2.6	47.0	1.72	1.2	53.0	1.62	2.8	98.8	2.98
15 January	2.6	41.7	1.53	1.3	72.3	1.51	2.8	99.2	3.01
1 February	2.6	36.4	1.30	1.3	76.4	1.47	2.8	99.3	3.04
15 February	2.6	33.4	1.19	1.3	82.2	1.45	2.8	99.5	3.08
1 March	2.6	31.6	1.10	1.3	83.2	1.43	2.8	99.5	3.11
15 March	2.4	35.5	1.13	1.3	86.3	1.34	2.8	99.5	3.14
1 April	2.6	54.7	1.02	1.3	89.1	1.29	2.8	99.5	3.18
15 April	2.8	79.3	0.96	1.3	87.0	1.33	2.8	99.5	3.21
29 April	2.8	88.9	1.01	1.2	90.6	1.36	2.8	99.5	3.23

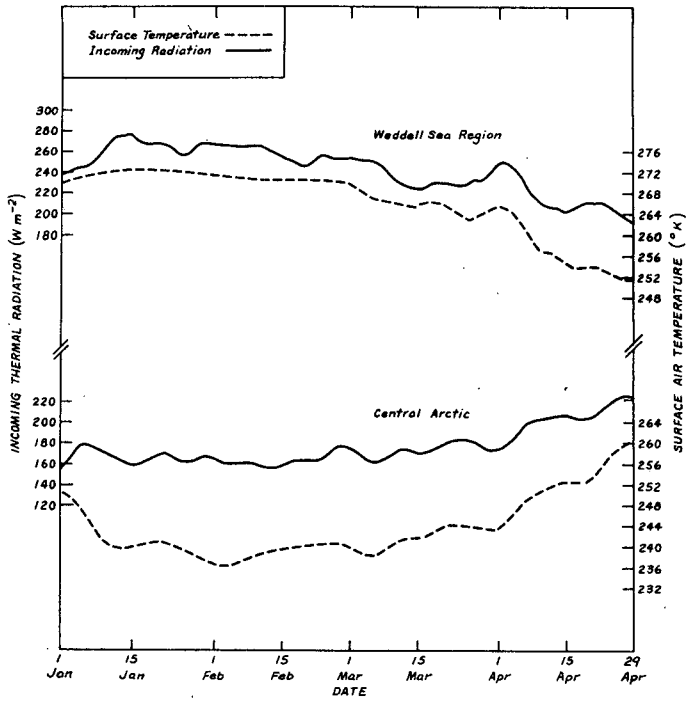

FIG. 8. GCM-generated surface temperature (broken line) and incoming longwave radiation for Weddell Sea Region (top) and Central Arctic Basin (bottom).

surface air temperatures and specific humidities, and the temperature and saturation vapor pressure produced by the ice model for the ice, snow and ocean surfaces. Thus, the surface fluxes are not interpreted as GCM fluxes, but rather as those fluxes which are mutually consistent with the respective temperatures generated by the ice and atmospheric models.

The evolution of the average GCM infrared radiation and surface temperature fields for the Weddell Sea region of the Southern Hemisphere is shown in the upper half of Fig. 8. Throughout most of January and February the surface air temperature is controlled by the melting sea ice, and remains near 272 K. The temperature decreases through March and April to 252 K, except for brief warmings which occur during mid March and early April. This behavior is in general agreement with the climatologies of surface stations near the Weddell Sea compiled by Schwerdtfeger (1970). Incoming longwave radiation during the first two months of the simulation period is about 260 W m^{-2} and decreases to 210–240 W m^{-2} during the latter two-month period, which is in general agreement with the zonal mean values obtained by Sasamori *et al.* (1972). Approximately 12 cm of snowfall (not shown) accumulates by the end of April.

The components of the Weddell Sea surface energy balance are shown in Fig. 9. GCM generated solar radiation is highly variable, and decreases from its 1 January value of 170 Wm^{-2} to 10 Wm^{-2} by the end of April. During the first half of the integration period the temperature difference between the air and ocean is small, and so consequently are the fluxes of sensible heat, latent heat and conduction. During most of this two-month period in the Weddell Sea the surface energy balance is governed largely by incoming radiation: The excess of solar radiation absorbed over net infrared radiation results in a warming of the ocean mixed layer and a decrease of ice volume, due to decreases in both thickness and concentration. During the latter half of the period the solar input becomes very small and the colder surface air temperatures are responsible for large evaporative and sensible heat fluxes from the ocean surface. The energy balance is strongly negative, and this is balanced jointly by ice accretion and further cooling of the mixed layer.

It is interesting to note how well the features of surface air temperature, surface energy fluxes, ice volume, and mixed layer temperature correlate with one another during March and April. For example, near the end of March there occurred in the GCM a brief warming of air temperatures and an increase in downwelling radiation. The regional response was rapid: Evaporation and convection from the surface diminished, ice accretion diminished and warming of the ice and ocean occurred. Clearly, evaporation and convection couple the ice model to the GCM in a rapid and efficient manner.

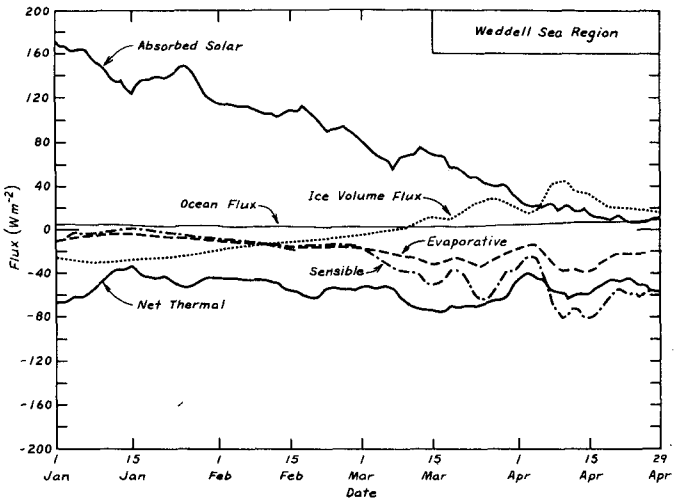

FIG. 9. Components of energy balance for ice in the Weddell Sea.

The smoothed GCM forcing parameters and resultant energy and mass budgets for the Central Arctic are shown in the lower half of Fig. 8 and in Fig. 10. Solar radiation is obviously irrelevant for the Central Arctic during most of this period. The incoming longwave radiation from the GCM is 160–180 Wm^{-2}, increasing toward the end of the integration period and agreeing reasonably well with the climatological values used by Maykut (1978). Approximately 24 cm of snow accumulated in the Central Arctic during this period, which is probably excessive. Observations show that typical wintertime accumulation is about 5 cm (Maykut and Untersteiner, 1971). Apparently this discrepancy did not cause any serious error in the simulated ice thickness. However, the melting of this excess snow would likely be a source of error if the integration were extended into the summer season. The GCM-generated Arctic surface air temperatures evolve in a realistic way as compared with observed climatologies (cf., Vowinckel and Orvig, 1970).

The components of the surface energy balance in the Central Arctic behave in a relatively simple fashion during this period. The evaporative heat flux is essentially zero because of the cold temperatures and resultant low atmospheric moisture capacity. The longwave energy lost from the surface is almost entirely compensated for by the sensible heat gained from the atmosphere and the energy conducted up from the ocean. The time series of sensible heat and radiative fluxes are similar to one another, and this again illustrates the strong coupling between GCM-generated radiation fields and ice model generated surface temperatures. The net energy loss

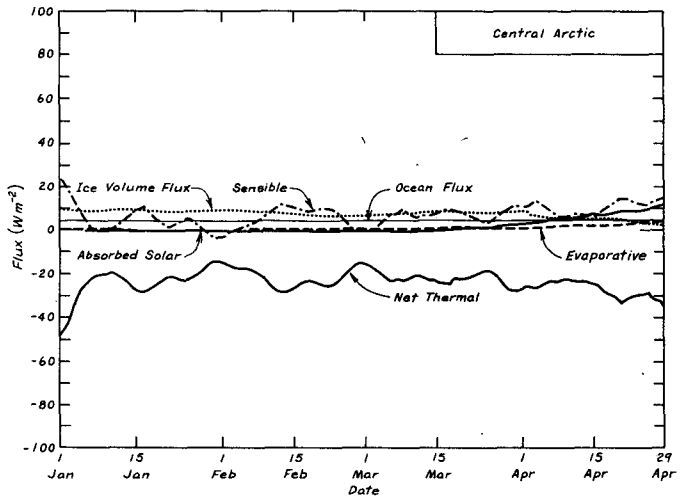

FIG. 10. Components of energy balance for ice in the Central Arctic.

from the entire layer of ice is about 10 Wm^{-2}, and this results in the accretion of about 18 cm of ice.

5. Summary and conclusions

The results of these experiments provide a number of useful insights into the problem of constructing coupled atmosphere-ice-ocean general circulation models. Most significantly, it appears that the GLAS GCM is capable of generating atmospheric fields in the Arctic and Antarctic that are sufficiently precise and accurate to produce reasonable distributions of sea ice when used in conjunction with a thermodynamic sea ice model. This conclusion is of course limited to the four-month period investigated. Systematic errors in the GCM's radiation were originally a source of concern given the typical sensitivity (e.g., Maykut and Untersteiner, 1971) of thermodynamic ice models to anomalies in the atmospheric fluxes. Also unknown was the response of the ice model to the large variations in atmospheric fluxes that occur in the GCM from time step to time step and from grid point to grid point. The ice model proves fairly insensitive to these nearly random fluctuations, and in fact integrates them into relatively smooth distributions of ice thickness and concentration. Obviously the effect of *systematic* errors will be a source of concern as the integration time of the GLAS GCM is extended to several seasons or years.

Most encouraging was the success in simulating the gross variations of the sea ice concentration in the Central Arctic, East Greenland Sea, Barents Sea, and Bering Sea sectors. Ice thickness in the Central Arctic agrees reasonably well with the observed average thickness of 3 m. The spatial trend recently reported by Hibler (1979) was not incorporated in the initial conditions and did not appear in the results. Perhaps a longer simulation and the incorporation of ice dynamics would produce these spatial variations.

The summer decay season of the ice simulated in the Antarctic extends several weeks beyond the normal observed ice minimum. This unrealistic behavior of the ice in the Southern Hemisphere is probably related to GCM errors in the high southern latitudes (Herman and Johnson, 1980), since the same sea ice model has demonstrated reasonable behavior in the Antarctic when forced with observed climatological data (Parkinson and Washington, 1979). The GCM-driven simulation does reproduce the fall-season extension of the ice, the major difficulty being simply that this growth is delayed for several weeks in early March.

The sensitivity of ice thermodynamics to the incoming radiation fields is troublesome. The solar and thermal fluxes generated by a GCM depend on the radiation model employed and, equally importantly, on a set of difficult-to-measure empirical parameters that determine atmospheric absorption. These include gaseous transmission, aerosol content and aerosol optical properties, cloudiness and cloud optical properties. The large uncertainty in measuring Arctic stratus cloud absorptance, for example, has been noted by Herman (1977), and one limit to the predictability of ice thickness is clearly imposed by such uncertain atmospheric parameters. The effect of systematic errors in the GCM-generated surface air temperatures and specific humidities, as well as in snowfall rates, remains to be investigated.

The ice model utilized here is principally a thermodynamic model; later experiments will be conducted with versions that will account for ice dynamics and mechanics, and the salinity structure of the oceanic mixed layer. Before successful fully coupled simulations are understood there are a range of sensitivity experiments that need to be conducted with these various models for integration periods extending to several seasons or years.

Acknowledgments. We are indebted to Drs. M. Halem and H. J. Zwally for providing the resources and facilities that were necessary for these experiments. The programming support of Messrs. M. Good and W. Johnson is especially acknowledged. G. F. Herman is supported at the University of Wisconsin under NASA Grant NSG-5152.

REFERENCES

Bryan, K., S. Manabe, and R. C. Pacanowski, 1975: A global ocean-atmosphere climate model. Part II. The oceanic circulation. *J. Phys. Oceanogr.*, **5**, 30–46.

Corby, G. A., A. Gilchrist, and R. L. Newson, 1972: A general circulation model of the atmosphere suitable for long period integrations. *Quart. J. Roy. Meteor. Soc.*, **98**, 809–832.

Halem, M., J. Shukla, Y. Mintz, M. L. Wu, R. Godbole, G. Herman, and Y. Sud, 1979: Comparison of observed seasonal climate features with a winter and summer numerical simulation produced with the GLAS general circulation model. Report of the JOC Study Conf. on Climate Models: Performance, Intercomparison and Sensitivity Studies, *GARP Publ. Series No. 22*, 207–253, WMO, Geneva, Switzerland.

Herman, G. F., 1977: Solar radiation in Arctic stratus clouds. *J. Atmos. Sci.*, **34**, 1423–1432.

Herman, G. F., and W. T. Johnson, 1978: The sensitivity of the general circulation to Arctic sea ice boundaries: A numerical experiment. *Mon. Wea. Rev.*, **106**, 1649–1664.

Herman, G. F., and W. T. Johnson, 1980: Arctic and Antarctic climatology of the GLAS General Circulation Model. *Mon. Wea. Rev.*, **108**, 1974–1991.

Hibler, W. D., III, 1979: A dynamic thermodynamic sea ice model. *J. Phys. Oceanog.*, **9**, 815–846.

Lacis, A. A., and J. E. Hansen, 1974: A parameterization for the absorption of solar radiation in the earth's atmosphere. *J. Atmos. Sci.*, **31**, 118–133.

Ling, C. H., L. A. Rasmussen, and W. J. Campbell, 1980: A continuum sea ice model for a global climate model. *Sea Ice Processes and Models*, R. Pritchard, Ed., University of Washington Press, 187–196.

Manabe, S., K. Bryan, and M. J. Spelman, 1975: A global ocean-atmosphere climate model. Part I. The atmospheric circulation. *J. Phys. Oceanogr.*, **5**, 3–29.

Manabe, S., K. Bryan, and M. J. Spelman, 1979: A global ocean-atmosphere climate model with seasonal variation for future

studies of climate sensitivity. *Dyn. Atmos. Oceans,* **3,** 393–426.

Manabe, S., and R. T. Wetherald, 1980: On the distribution of climate change resulting from an increase in CO_2 content of the atmosphere. *J. Atmos. Sci.,* **37,** 99–118.

Maykut, G. A., 1978: Energy exchange over young sea ice in the Central Arctic. *J. Geophys. Res.,* **83,** 3646–3658.

Maykut, G. A., and N. Untersteiner, 1971: Some results from a time-dependent, thermodynamic model of sea ice. *J. Geophys. Res.,* **76,** 1550–1575.

Parkinson, C. L., and W. M. Washington, 1979: A large-scale numerical model of sea ice. *J. Geophys. Res.,* **84,** 311–337.

Pritchard, R. S., M. D. Coon, and M. G. McPhee, 1977: Simulation of sea ice dynamics during AIDJEX. *J. Pressure Vessel Tech.,* **99,** 491–497.

Rothrock, D. A., 1975: The steady drift of an incompressible Arctic ice cover. *J. Geophys. Res.,* **80,** 387–397.

Saltzman, B., 1978: A survey of statistical-dynamical models of the terrestrial climate. *Advances in Geophysics,* Vol. 20, Academic Press, 184–295.

Sasamori, T., J. London, and D. Hoyt, 1972: Radiation budget of the Southern Hemisphere. *Meteor. Monogr.,* No. 35, Amer. Meteor. Soc., 9–22.

Schlesinger, M. E., and W. L. Gates, 1979: Performance of the Oregon State University two-level atmospheric general circulation model. Report of the JOC Study Conf. on Climate Models: Performance, Intercomparison and Sensitivity Studies, *GARP Publ. Series No. 22,* 139–206, WMO, Geneva, Switzerland.

Schwerdtfeger, W., 1970: The climate of the Antarctic. In: *World Survey of Climatology,* Vol. 14, *Climates of the Polar Regions.* S. Orvig, Ed., Elsevier, 370 pp.

Semtner, A. J., Jr., 1976: A model for the thermodynamic growth of sea ice in numerical investigations of climate. *J. Phys. Oceanogr.,* **6,** 379–389.

Stone, P. H., S. Chow, and W. J. Quirk, 1977: The July climate and a comparison of the January and July climates simulated by the GISS general circulation model. *Mon. Wea. Rev.,* **105,** 170–194.

Somerville, R. C. J., P. H. Stone, M. Halem, J. E. Hansen, J. S. Hogan, L. M. Druyan, G. Russell, A. A. Lacis, W. J. Quirk, and J. Tenenbaum, 1974: The GISS model of the global atmosphere. *J. Atmos. Sci.,* **31,** 84–117.

Vowinckel, E. and S. Orvig, 1970: The climate of the north polar basin. In: *World Survey of Climatology,* Vol. 14, *Climates of the Polar Regions.* S. Orvig, Ed., Elsevier, 370 pp.

Walsh, J. E., and C. M. Johnson, 1979: Interannual atmospheric variability and associated fluctuations in Arctic sea ice extent. *J. Geophys. Res.,* **84,** 6915–6928.

Warshaw, M., and R. R. Rapp, 1973: An experiment on the sensitivity of a global circulation model. *J. Appl. Meteor.,* **12,** 43–49.

Washington, W. M., A. J. Semtner, Jr., C. L. Parkinson, and L. Morrison, 1976: On the development of a seasonal change sea ice model. *J. Phys. Oceanogr.,* **6,** 679–685.

Washington, W. M., A. J. Semtner, Jr., G. A. Meehl, D. J. Knight, and T. A. Mayer, 1980: A general circulation experiment with a coupled atmosphere, ocean and sea ice model. *J. Phys. Oceanogr.,* **10** (in press).

Washington, W. M., and D. L. Williamson, 1977: A description of the NCAR global circulation models. *Methods in Computational Physics,* Vol. 17, *General Circulation Models of the Atmosphere,* J. Chang, Ed., Academic Press, 111–172.

Williams, J., R. G. Barry, and W. M. Washington, 1974: Simulation of the atmosphere using the NCAR global circulation model with Ice Age boundary conditions. *J. Appl. Meteor.,* **13,** 305–317.

Wu, M. L., 1980: The exchange of infrared radiative energy in the troposphere. *J. Geophys. Res.,* **85,** 4084–4090.

Zwally, H. J., and P. Gloersen, 1977: Passive microwave images of the polar regions and research applications. *Polar Record,* **18,** 431–450.